

Microwave Linear Analog Computer (MiLAC)-Aided MIMO Radar Sensing: Transmit Beamforming Design and DoA Estimation

Ziang Liu, Zheyu Wu, and Bruno Clerckx, *Fellow, IEEE*

Abstract—Multiple-input multiple-output (MIMO) radar has waveform diversity and large spatial degrees of freedom (DoFs), making it attractive for high-resolution sensing. Scaling MIMO radar to massive arrays can further improve sensing performance, but it also increases hardware cost, power consumption, and digital processing complexity. The microwave linear analog computer (MiLAC) can tackle these challenges by moving linear operations from the digital domain to the analog domain. MiLAC has shown promising benefits for communications in recent studies and this paper identifies its potential for radar sensing. Specifically, we consider both MiLAC-aided transmit beamforming and receiver-side two-dimensional discrete Fourier transform (2D-DFT)-based direction-of-arrival (DoA) estimation. For transmit beamforming, we formulate a weighted Cramér-Rao bound (CRB) minimization problem under lossless and reciprocal MiLAC constraints and propose a penalty dual decomposition (PDD)-based iterative algorithm to address the non-convex problem. We further prove that MiLAC-aided and fully-digital beamforming achieve the same CRB. For receiver processing, we show that the 2D DFT can be implemented by a lossless reciprocal MiLAC, which enables analog-domain DoA estimation without digital optimization. Numerical results confirm the theoretical finding and show that the MiLAC-aided approach achieves the same CRB and DoA estimation performance as the fully-digital benchmark. Meanwhile, hardware cost and power consumption are reduced because only low-resolution DACs are required at the transmitter, while RF chains and ADCs are eliminated at the receiver. Moreover, performing the 2D DFT in the analog domain eliminates all digital DFT operations for DoA estimation.

Index Terms—Analog computation, Cramér-Rao bound (CRB), direction-of-arrival (DoA) estimation, Microwave linear analog computer (MiLAC), MIMO radar.

I. INTRODUCTION

Sensing is expected to be a core functionality of future wireless systems [1]. Among sensing technologies, multiple-input multiple-output (MIMO) radar is particularly attractive because multiple antennas and multiple orthogonal waveforms provide large spatial degrees of freedom (DoFs) and waveform diversity compared with phased-array radar [2], [3]. These DoFs bring gains in beam pattern design, target detection, parameter estimation [3]–[5], and interference suppression [6]. As a result, MIMO radar has been adopted in applications such as automotive radar [7], remote sensing [8], and integrated sensing and communication [9]. Extending MIMO radar to massive arrays is a natural step toward higher spatial resolution

and larger array gain [10], [11], and it has motivated substantial recent interest in mm-wave [12] and terahertz (THz) [13] massive MIMO radar systems.

However, this scaling creates two bottlenecks. The first is *hardware cost* and *power consumption*. Fully exploiting the DoFs of a MIMO radar requires one RF chain per antenna, including DACs and ADCs, which dominate the overall power consumption [14]. For example, a 256-antenna array using 12-bit ADCs at 20 Gsamples/s can consume 256 W [15], which is difficult to sustain in practical deployments. The second bottleneck is *computational complexity*. As the array size increases, the computational complexity of digital transmit beamforming and receiver-side parameter estimation grows substantially. Even discrete Fourier transform (DFT)-based digital processing incurs non-negligible complexity. In addition, subspace-based methods such as multiple signal classification (MUSIC) additionally requires eigenvalue decompositions and matrix inversions, resulting in complexity at the order of $\mathcal{O}(N^3)$ [16]. For latency-sensitive applications such as automotive radar, this digital processing burden can become prohibitive.

Existing approaches typically address only part of this problem. To reduce hardware cost and power consumption, low-resolution DACs/ADCs architectures have been studied, because the power consumption of DACs/ADCs scales exponentially with quantization resolution [14]. At the extreme, 1-bit DACs/ADCs substantially simplify the transceiver, and have been considered for MIMO radar waveform design, detection, parameter estimation, and tracking [17]–[20]. While such designs can be attractive, the information loss introduced by coarse quantization is irreversible and can significantly degrade sensing performance. Hybrid analog-digital beamforming is another route by reducing the number of RF chains, but the resulting reduction in waveform diversity and beamforming flexibility causes performance loss compared to fully-digital architectures [21]. Another alternative is to move beamforming entirely to the analog domain, thus allowing the RF chains to directly carry radar-modulated signals, *e.g.*, frequency-modulated continuous-wave (FMCW) waveforms. Therefore, only low-resolution DACs/ADCs are required, which can reduce hardware cost and power consumption. Stacked intelligent metasurfaces (SIMs), which are realized by cascaded transmissive RIS layers, are a representative example of this direction [22]. Specifically, the 2D DFT-based DoA estimation is achieved by SIMs and directly in the analog domain [22].

Analog-domain processing is also advantageous from a computational complexity perspective. Over-the-air computa-

Z. Liu, Z. Wu, and B. Clerckx are with the Communications & Signal Processing (CSP) Group at the Dept. of Electrical and Electronic Engg., Imperial College London, SW7 2AZ, UK. (e-mails: {ziang.liu20}@imperial.ac.uk).

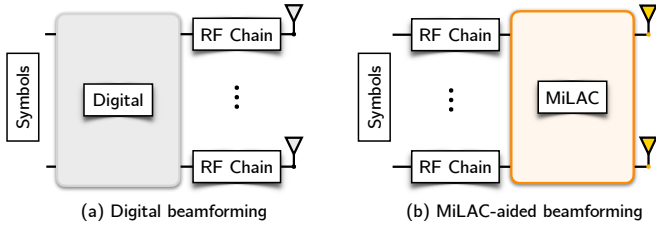


Fig. 1. Comparison between (a) digital beamforming and (b) MiLAC-aided analog beamforming.

tion (OAC) exploits the property of electromagnetic (EM) waveform superposition to realize efficient computation during transmission. In addition, this method has been employed for data aggregation in integrated sensing and communication systems [23], [24]. However, its supported operations are mainly limited to nomographic functions such as weighted sums and arithmetic means [23]. For more general linear transforms, SIM-aided analog computing has recently been proposed for tasks such as transmit beamforming design and DFT realization [25]–[27]. However, analog domain processing typically decreases the flexibility and thus leads to performance loss compared to digital processing due to the operations are on the microwave impedance network [28].

So far a unified framework of analog computation is missing, but microwave linear analog computer (MiLAC) provides a first promising attempt [28]. Built on multiport microwave networks with reconfigurable impedance components, MiLAC implements linear transformations directly in the analog domain (cf. Fig. 1) by tuning the impedance network [28], [29]. Recent work has shown that MiLAC supports purely analog linear zero-forcing beamforming (ZFZF) and minimum mean square error (LMMSE)-based transmit and receive beamforming for MIMO communications [28], [29]. A physics-compliant model considering mutual coupling is investigated in [30], showing that mutual coupling is on average beneficial in MiLAC-aided systems. To alleviate the high circuit complexity and control overhead, [31] proposes a one-layer stem-connected MiLAC architecture that preserves capacity-achieving performance in single-user MIMO systems while significantly reducing hardware complexity. Analog-domain channel estimation is proposed in [32], achieving the same performance as its digital-domain counterpart while reducing computational complexity and hardware requirements.

From a hardware perspective, losslessness and reciprocity are common constraints for microwave impedance networks. Under these constraints, MiLAC-aided beamforming can match the capacity of fully-digital beamforming in point-to-point MIMO communication systems [33]. For multi-user communications, [34], [35] further show that MiLAC does not in general retain the full flexibility of digital beamforming, but a hybrid digital-MiLAC architecture can achieve maximum performance with only K RF chains for K users, whereas conventional hybrid beamforming requires $2K$ [36]. More recently, [37] shows that a two-layer reciprocal and lossless MiLAC achieves the same performance as fully-digital beamforming in multi-user MISO systems, and [38] studies

hybrid digital-MiLAC beamforming for wideband multi-user (MU) MIMO systems, demonstrating that the proposed design consistently outperforms conventional hybrid digital-analog beamforming. To summarize, MiLAC-aided communications has shown the following promising benefits: 1) *MiLAC offers the same flexibility as digital beamforming, and hence achieves maximum performance.* 2) *MiLAC requires only as many RF chains as the number of transmitted symbols, i.e., data streams.* Since the signals carried and sampled at the RF chains are the actual symbols, 3) *low-resolution ADCs and DACs are sufficient.* 4) *MiLAC does not require any computation at each symbol time, since the symbols are precoded and combined fully in the analog domain.* 5) *MiLAC can perform ZFBF and MMSE combining with significantly reduced computational complexity, i.e., $\mathcal{O}(N^2)$ instead of $\mathcal{O}(N^3)$.*

However, these results focus on communication systems. The use of MiLAC for MIMO radar sensing, especially under practical lossless and reciprocal constraints, remains unexplored. Recent prototype-level evidence shows that hybrid couplers and phase shifters can realize linear transforms, i.e., a 4×4 DFT [39], further motivating the study of MiLAC for radar sensing. In radar systems, scaling to massive arrays increases not only hardware cost and power consumption due to high-resolution DACs and RF chains, but also computational complexity due to large-dimensional DFT operations for DoA estimation. To address these challenges, this paper investigates MiLAC-aided MIMO radar for the first time from both the transmitter and receiver sides. Under lossless and reciprocal constraints, we show that MiLAC-aided radar sensing has the following benefits. 1) *MiLAC achieves the same sensing performance as fully-digital beamforming, since the set of achievable transmit covariance matrices under MiLAC constraints is identical to that of fully-digital beamforming, and the Cramér–Rao bound (CRB) depends on the beamforming matrix only through the transmit covariance (See Section III-B).* In addition, the 2D DFT-based DoA estimation can be exactly implemented by a lossless reciprocal MiLAC (See Section IV). 2) *MiLAC reduces hardware cost and power consumption, because MiLAC enables fully analog beamforming and thus the RF chains can directly carry radar-modulated signals with lower-resolution DACs/ADCs.* 3) *MiLAC requires no per-symbol digital processing, as the transmit beamforming in MIMO radar is entirely implemented in the analog domain.* 4) *DFT-based DoA estimation can be achieved with minimum computational complexity, because the DFT can be exactly implemented by a lossless reciprocal MiLAC without any offline optimization.* 5) *Ultra-low latency especially in massive MIMO radar due to that the DFT is performed in the analog domain.* This is particularly beneficial for real-time detection and tracking applications such as automotive radar. These advantages make MiLAC especially appealing for massive array and real-time radar applications.

Contributions and Overview of Results. The main contributions of this paper are summarized as follows:

- 1) This is the first work to investigate MiLAC-aided MIMO radar sensing under practical lossless and reciprocal constraints. Specifically, we formulate transmit beamforming

for MiLAC-aided MIMO radar as a weighted CRB minimization problem for multi-target 2D angle estimation, under both the total transmit power constraint and the lossless reciprocal constraints imposed by the MiLAC impedance network. On the receiver side, we show that the 2D DFT can be implemented by a lossless reciprocal MiLAC, which enables analog-domain DoA estimation without offline digital optimization.

- 2) We prove that MiLAC-aided and fully-digital beamforming achieve the same optimal CRB. The key insight is that the CRB depends on the beamforming matrix only through the transmit covariance, and we show that the set of achievable transmit covariance matrices is identical under both architectures.
- 3) We develop a penalty dual decomposition (PDD)-based iterative algorithm [40] to solve the non-convex transmit beamforming problem. The algorithm alternately updates the beamforming matrix, power allocation vector, and auxiliary variable until convergence.
- 4) Numerical results confirm that the proposed MiLAC-aided beamforming design achieves the same CRB as fully-digital beamforming and can probe the beams at the target angles. On the receiver side, MiLAC-aided 2D-DFT DoA estimation achieves the same performance as fully-digital DFT-based DoA estimation. Furthermore, the receiver-side computational complexity of 2D-DFT-based DoA estimation is significantly reduced by MiLAC, especially for large arrays. These gains in sensing performance are obtained with lower hardware cost and computational complexity compared to fully-digital approaches.
- 5) Overall, under lossless and reciprocal constraints, we show that 1) MiLAC achieves the same sensing performance as fully-digital beamforming, 2) MiLAC reduces hardware cost and power consumption, 3) MiLAC requires no per-symbol digital processing, 4) DFT-based DoA estimation can be achieved with minimum computational complexity, and 5) Ultra-low latency especially in massive MIMO radar.

Organization of This Paper. Section II presents the sensing system model, the MiLAC model, and the MiLAC-aided signal processing at the transmitter and receiver. Section III explains the transmit-side beamforming design, including the multi-target CRB derivation, the weighted CRB minimization problem, and the proposed algorithm with its convergence and complexity analysis. Section IV addresses receiver-side MiLAC-aided 2D-DFT-based DoA estimation. Numerical results are given in Section V, and conclusions are drawn in Section VI.

Notation. The sets of integers, real numbers, and complex numbers are denoted by \mathbb{Z} , \mathbb{R} , and \mathbb{C} , respectively. Matrices, vectors, and scalars are represented by bold uppercase, bold lowercase, and regular fonts, respectively. The real part of a complex number is denoted by $\Re(\cdot)$. For $x \in \mathbb{R}$, we define the ceiling operations by $\lceil x \rceil = \inf\{k \in \mathbb{Z} : k \geq x\}$. For a matrix \mathbf{X} , its transpose, conjugate-transpose, and inverse are denoted by \mathbf{X}^\top , \mathbf{X}^H , and \mathbf{X}^{-1} , respectively. The element in the i^{th} row and j^{th} column of the matrix \mathbf{X} is denoted by $[\mathbf{X}]_{i,j}$. The

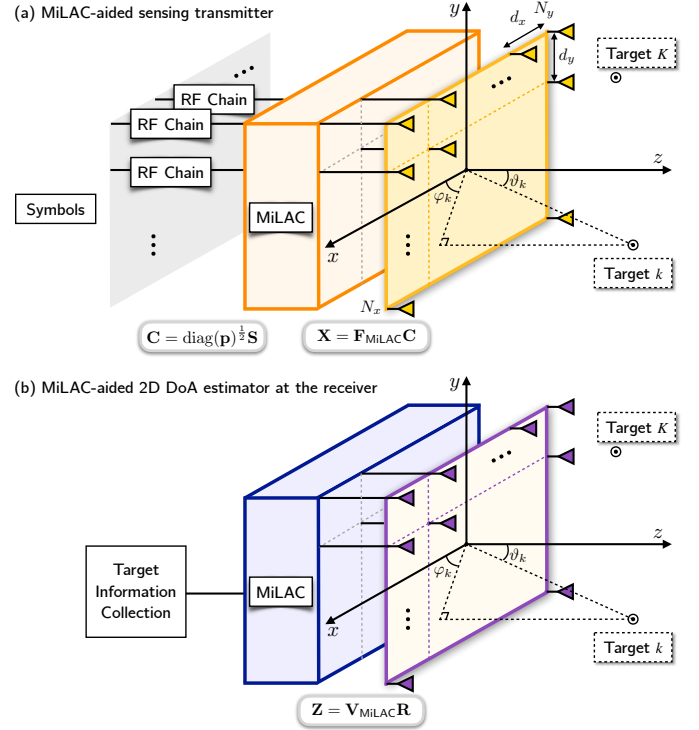


Fig. 2. Architecture of the MiLAC-aided sensing system.

identity matrix and all-zero matrix are represented by \mathbf{I} and $\mathbf{0}$. The diagonal matrix, and trace operation are denoted by $\text{diag}(\cdot)$ and $\text{tr}(\cdot)$, respectively. The absolute value, statistical expectation, Kronecker product and Hadamard (element-wise) product are denoted by $|\cdot|$, $\mathbb{E}(\cdot)$, \otimes and \odot , respectively.

II. SYSTEM MODEL

A. Sensing System Model

As shown in Fig. 2, the co-located transmit and receive antenna uniform planar arrays (UPA) are assumed to have $N = N_x N_y$ antennas, where N_x and N_y are the number of elements in x -direction and y -direction, respectively. The element spacings are d_x and d_y . Let K denote the total number of targets. For the k^{th} target (where $k = 1, \dots, K$), $\varphi_k \in [0, 2\pi)$ and $\vartheta_k \in [0, \pi/2]$ denote the azimuth angle and elevation angle of the signal relative to the antenna arrays. Thus, the electrical angles $\psi_{x,k}$ and $\psi_{y,k}$ in the x - and y -directions for the k^{th} target are given by

$$\psi_{x,k} = \kappa d_x \sin(\vartheta_k) \cos(\varphi_k), \quad \psi_{y,k} = \kappa d_y \sin(\vartheta_k) \sin(\varphi_k), \quad (1)$$

where $\kappa = 2\pi/\lambda$ denotes the wavenumber and λ is the wavelength.

The steering vectors with respect to (w.r.t) the transmit and receive antenna arrays for the k^{th} target are represented by $\mathbf{a}(\psi_{x,k}, \psi_{y,k}) \in \mathbb{C}^{N \times 1}$ and $\mathbf{b}(\psi_{x,k}, \psi_{y,k}) \in \mathbb{C}^{N \times 1}$, respectively [41], where

$$\mathbf{a}(\psi_{x,k}, \psi_{y,k}) \triangleq \mathbf{a}_y(\psi_{y,k}) \otimes \mathbf{a}_x(\psi_{x,k}) \quad (2)$$

$$\mathbf{b}(\psi_{x,k}, \psi_{y,k}) \triangleq \mathbf{a}_y(\psi_{y,k}) \otimes \mathbf{a}_x(\psi_{x,k}). \quad (3)$$

The elements of the vectors $\mathbf{a}_x(\psi_{x,k}) \in \mathbb{C}^{N_x \times 1}$ and $\mathbf{a}_y(\psi_{y,k}) \in \mathbb{C}^{N_y \times 1}$ are defined as follows:

$$[\mathbf{a}_x(\psi_{x,k})]_{n_x} \triangleq e^{j\psi_{x,k}(n_x-1)}, \quad n_x = 1, \dots, N_x, \quad (4)$$

$$[\mathbf{a}_y(\psi_{y,k})]_{n_y} \triangleq e^{j\psi_{y,k}(n_y-1)}, \quad n_y = 1, \dots, N_y. \quad (5)$$

The n^{th} antenna element has the coordinates (n_x, n_y) , where n_x and n_y are the indices of the antenna element in the x - and y -directions, respectively, given by

$$n_y \triangleq \lceil n/N_x \rceil, \quad n_x \triangleq n - (n_y - 1)N_x. \quad (6)$$

Let $\mathbf{A}_k(\psi_{x,k}, \psi_{y,k}) \triangleq \mathbf{b}(\psi_{x,k}, \psi_{y,k})\mathbf{a}^\top(\psi_{x,k}, \psi_{y,k})$ denote the round-trip steering matrix of target k . The received signal $\mathbf{R} \in \mathbb{C}^{N \times L}$ at the receive UPA, after reflection from the K targets, can be expressed as

$$\begin{aligned} \mathbf{R} &= \sum_{k=1}^K \alpha_{r,k} \mathbf{b}(\psi_{x,k}, \psi_{y,k}) \mathbf{a}^\top(\psi_{x,k}, \psi_{y,k}) \mathbf{F}_{\text{MiLAC}} \text{diag}(\mathbf{p})^{\frac{1}{2}} \mathbf{S} + \mathbf{N} \\ &= \sum_{k=1}^K \alpha_{r,k} \mathbf{A}_k(\psi_{x,k}, \psi_{y,k}) \mathbf{F}_{\text{MiLAC}} \mathbf{C} + \mathbf{N}, \end{aligned} \quad (7)$$

where $\alpha_{r,k}$ denotes the reflection coefficient of the k^{th} target, which captures both the round-trip path loss and the radar cross-section (RCS). Let M denote the number of waveforms and L the snapshot length. $\mathbf{F}_{\text{MiLAC}} \in \mathbb{C}^{N \times M}$ is the input-output transfer matrix of the MiLAC, as detailed in Section II-B. The transmitted signal is $\mathbf{X} = \mathbf{F}_{\text{MiLAC}} \mathbf{C}$, where $\mathbf{C} = \text{diag}(\mathbf{p})^{\frac{1}{2}} \mathbf{S} \in \mathbb{C}^{M \times L}$ is the source signal at the RF chains. Here, $\mathbf{p} \in \mathbb{R}^{M \times 1}$ with $p_m \geq 0$ for $m = 1, \dots, M$ denotes the power-allocation vector for the M waveforms, and $\mathbf{S} \in \mathbb{C}^{M \times L}$ is the known deterministic transmitted symbol matrix satisfying $\mathbf{S}\mathbf{S}^H = L\mathbf{I}$ [42]. Specifically, \mathbf{S} can be formed using phase-coded waveforms, where each waveform has constant modulus and different waveforms are orthogonal to one another, *e.g.*, using Hadamard codes [2]. Note that since the transmit beamforming is entirely in the analog domain, the RF chains directly carry the radar-modulated signals, which can be generated by low-resolution DACs. In addition, there is no per-symbol digital beamforming, which significantly reduces the computational complexity at the transmitter. The additive white Gaussian noise (AWGN) matrix is denoted by $\mathbf{N} \triangleq [\mathbf{n}[1], \mathbf{n}[2], \dots, \mathbf{n}[L]] \in \mathbb{C}^{N \times L}$, where $\mathbf{n}[t] \sim \mathcal{CN}(\mathbf{0}, \mathbf{I})$. We adopt $M = N$ such that the sensing signal achieves the full spatial DoFs (*i.e.*, $N^2 - N$) for target sensing [3], [4].

B. MiLAC Model

We consider a fully-connected MiLAC (cf. Fig. 3), where each pair of input and output ports is connected through a reconfigurable impedance and each port is also connected to ground through a reconfigurable impedance [28], [29], [34]. The input-output relationship of the $(N + M)$ -port MiLAC is characterized by $\mathbf{F}_{\text{MiLAC}} \in \mathbb{C}^{N \times M}$, and can be expressed as the scattering matrix $\Theta \in \mathbb{C}^{(N+M) \times (N+M)}$. The scattering matrix relates the incident and reflected waves at all ports and is obtained from the admittance matrix $\mathbf{Y} \in \mathbb{C}^{(N+M) \times (N+M)}$ via [33]

$$\Theta = (\mathbf{I} + Z_0 \mathbf{Y})^{-1} (\mathbf{I} - Z_0 \mathbf{Y}), \quad (8)$$

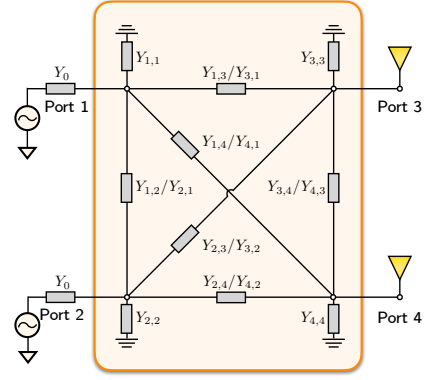


Fig. 3. A 4-port MiLAC with 2 input ports and 2 output ports. Reciprocal MiLAC means $Y_{i,j} = Y_{j,i}$.

where $Z_0 = 50 \Omega$ is the characteristic impedance. Following [34], the transfer matrix $\mathbf{F}_{\text{MiLAC}}$ is extracted from Θ as

$$\mathbf{F}_{\text{MiLAC}} = \frac{1}{2} [\Theta]_{M+1:M+N, 1:M}. \quad (9)$$

Subsequently, we impose two physical-compliant constraints on the microwave network, *i.e.*, *Losslessness* and *Reciprocity*. Specifically, losslessness requires that the network dissipates no energy, so that Θ is unitary. Reciprocity requires that the impedance between any two ports is identical in both directions, so that Θ is symmetric. Therefore, we have the following constraints:

$$\Theta^H \Theta = \mathbf{I}, \quad \Theta = \Theta^\top. \quad (10)$$

C. Transmit-side MiLAC-aided Beamforming

Using (9) and the lossless-reciprocal constraints, the set of achievable MiLAC-aided beamforming matrices is [34]

$$\begin{aligned} \mathcal{W}_{\text{MiLAC}} &= \{ \mathbf{W} = \mathbf{F} \text{diag}(\mathbf{p})^{\frac{1}{2}} \mid \mathbf{F} = [\Theta]_{M+1:M+N, 1:M}, \\ &\quad \Theta = \Theta^\top, \Theta^H \Theta = \mathbf{I}, \mathbf{1}^\top \mathbf{p} \leq P_T \}, \end{aligned} \quad (11)$$

where $\mathbf{F} \triangleq 2\mathbf{F}_{\text{MiLAC}}$ is introduced to simplify notation, and the factor of two is absorbed into the channel normalization. As shown in [34], the lossless and reciprocal constraints on the full scattering matrix Θ reduce to a spectral-norm constraint on the submatrix \mathbf{F} , yielding the equivalent characterization

$$\mathcal{W}_{\text{MiLAC}} = \{ \mathbf{W} = \mathbf{F} \text{diag}(\mathbf{p})^{\frac{1}{2}} \mid \|\mathbf{F}\|_2 \leq 1, \mathbf{1}^\top \mathbf{p} \leq P_T \}. \quad (12)$$

If we focus on the beamforming matrix \mathbf{W} , based on the Lemma 1 in [34], the set can be equivalently transformed to

$$\mathcal{W}_{\text{MiLAC}} = \{ \mathbf{W} \mid \mathbf{W}^H \mathbf{W} \preceq \text{diag}(\mathbf{p}), \mathbf{1}^\top \mathbf{p} \leq P_T \}. \quad (13)$$

Utilizing such set of MiLAC-aided beamforming matrices, we can design the transmit beamforming for MIMO radar sensing as shown in Fig. 2 (a).

D. Receiver-side MiLAC-aided Signal Processing

Beyond transmit beamforming, MiLAC can also perform receiver-side processing as shown in Fig. 2 (b). A second MiLAC with transfer matrix $\mathbf{V}_{\text{MiLAC}} \in \mathbb{C}^{N \times N}$ is placed

at the receiver and designed to implement the 2D DFT for DoA estimation. Since the DoA is directly on the analog-domain, RF chains and ADCs are not required, which can significantly reduce hardware cost and power consumption caused by ADCs. The resulting output is

$$\begin{aligned} \mathbf{Z} &= \mathbf{V}_{\text{MiLAC}} \mathbf{R} \\ &= \mathbf{V}_{\text{MiLAC}} \mathbf{A}(\psi_{x,k}, \psi_{y,k}) \mathbf{F}_{\text{MiLAC}} \mathbf{C} + \mathbf{V}_{\text{MiLAC}} \mathbf{N}. \end{aligned} \quad (14)$$

Considering the lossless and reciprocal constraints, the feasible set for the receiver-side MiLAC is [28], [29], [33], [34]

$$\left\{ \mathbf{V}_{\text{MiLAC}} \mid \mathbf{V}_{\text{MiLAC}} = \frac{1}{2} [\boldsymbol{\Theta}]_{N+1:2N, 1:N}, \boldsymbol{\Theta} = \boldsymbol{\Theta}^\top, \boldsymbol{\Theta}^H \boldsymbol{\Theta} = \mathbf{I} \right\} \quad (15)$$

III. TRANSMIT-SIDE MiLAC-AIDED BEAMFORMING: PROBLEM FORMULATION AND SOLUTION

In this section, we first derive the CRB for 2D multi-target angle estimation, which serves as the performance metric for sensing. Subsequently, we formulate the transmit beamforming optimization problem for MiLAC-aided MIMO radar sensing under power constraint, and lossless and reciprocal constraints. In addition, we consider the digital beamforming design as a benchmark for performance comparison.

A. Cramér Rao Bound for 2D Sensing

Sensing performance is characterized by the Cramér Rao bound (CRB), which gives a lower bound on the mean square error (MSE) achievable by any unbiased estimator [43]. The CRB is determined by the likelihood of the raw observation \mathbf{R} in (7), not by specific post-processing applied to it [43], *e.g.*, designing $\mathbf{V}_{\text{MiLAC}}$ to realize DFT-based DoA detection in our case. Consequently, the CRB depends only on the transmit beamforming matrix \mathbf{W} and is independent of $\mathbf{V}_{\text{MiLAC}}$. Let \mathbf{J} denote the Fisher information matrix (FIM). Then, the CRB matrix is given by $\boldsymbol{\Xi} = \mathbf{J}^{-1}$. For K targets, define the unknown parameter vector as

$$\boldsymbol{\xi} = [\boldsymbol{\theta}^\top, \boldsymbol{\alpha}^\top]^\top \in \mathbb{R}^{4K \times 1}, \quad (16)$$

where $\boldsymbol{\theta} \triangleq [\boldsymbol{\theta}_1^\top, \dots, \boldsymbol{\theta}_K^\top]^\top$ collects the target angles with $\boldsymbol{\theta}_k \triangleq [\vartheta_k, \varphi_k]^\top$, and $\boldsymbol{\alpha} \triangleq [\boldsymbol{\alpha}_1^\top, \dots, \boldsymbol{\alpha}_K^\top]^\top$ collects the real and imaginary parts of the radar cross-section (RCS), with $\boldsymbol{\alpha}_k \triangleq [\Re\{\alpha_{r,k}\}, \Im\{\alpha_{r,k}\}]^\top$.

Based on (7), the noise-free received signal is

$$\begin{aligned} \boldsymbol{\mu} &= \sum_{k=1}^K \alpha_{r,k} \mathbf{A}_k(\psi_{x,k}, \psi_{y,k}) \mathbf{F}_{\text{MiLAC}} \text{diag}(\mathbf{p})^{\frac{1}{2}} \mathbf{S} \\ &= \frac{1}{2} \sum_{k=1}^K \alpha_{r,k} \mathbf{A}_k(\psi_{x,k}, \psi_{y,k}) \mathbf{W} \mathbf{S} = \mathbf{A} \mathbf{W} \mathbf{S}, \end{aligned} \quad (17)$$

where $\mathbf{W} \in \mathcal{W}_{\text{MiLAC}}$, and the composite round-trip steering matrix is defined as

$$\mathbf{A} \triangleq \frac{1}{2} \sum_{k=1}^K \alpha_{r,k} \mathbf{A}_k(\psi_{x,k}, \psi_{y,k}) \in \mathbb{C}^{N \times N}. \quad (18)$$

The factor of $\frac{1}{2}$ arises because the transmit power constraint is imposed on the voltage-generator signal \mathbf{C} , not on the antenna

signal \mathbf{X} . Specifically, under perfect matching to the source impedance Z_0 , the radiated signal is $\mathbf{X} = \mathbf{C}/2$ [33].¹

Since each parameter ξ_i belongs to a specific target k , and only \mathbf{A}_k depends on the parameters of target k , the derivatives of $\boldsymbol{\mu} = \mathbf{A} \mathbf{W} \mathbf{S}$ w.r.t. target k are given by

$$\frac{\partial \boldsymbol{\mu}}{\partial \vartheta_k} = \frac{\partial \mathbf{A}}{\partial \vartheta_k} \mathbf{W} \mathbf{S} = \frac{1}{2} \alpha_{r,k} \dot{\mathbf{A}}_{\vartheta_k} \mathbf{W} \mathbf{S}, \quad (19a)$$

$$\frac{\partial \boldsymbol{\mu}}{\partial \varphi_k} = \frac{\partial \mathbf{A}}{\partial \varphi_k} \mathbf{W} \mathbf{S} = \frac{1}{2} \alpha_{r,k} \dot{\mathbf{A}}_{\varphi_k} \mathbf{W} \mathbf{S}, \quad (19b)$$

$$\frac{\partial \boldsymbol{\mu}}{\partial \alpha_k} = \frac{\partial \mathbf{A}}{\partial \alpha_k} \mathbf{W} \mathbf{S} = [1 \quad j]^\top \otimes \frac{1}{2} \mathbf{A}_k \mathbf{W} \mathbf{S}, \quad (19c)$$

where $\dot{\mathbf{A}}_{\vartheta_k} \triangleq \frac{\partial \mathbf{A}_k}{\partial \vartheta_k}$ and $\dot{\mathbf{A}}_{\varphi_k} \triangleq \frac{\partial \mathbf{A}_k}{\partial \varphi_k}$ denote the derivatives of the per-target round-trip steering matrix w.r.t. the elevation and azimuth angles, respectively. Their explicit expressions are provided in Appendix A.

For estimating $\boldsymbol{\xi}$ from L observations, the FIM has the block structure [43]

$$\mathbf{J} = \begin{bmatrix} \mathbf{J}_{\boldsymbol{\theta}\boldsymbol{\theta}} & \mathbf{J}_{\boldsymbol{\theta}\boldsymbol{\alpha}} \\ \mathbf{J}_{\boldsymbol{\theta}\boldsymbol{\alpha}}^\top & \mathbf{J}_{\boldsymbol{\alpha}\boldsymbol{\alpha}} \end{bmatrix}. \quad (20)$$

The submatrices $\mathbf{J}_{\boldsymbol{\theta}\boldsymbol{\theta}} \in \mathbb{R}^{2K \times 2K}$, $\mathbf{J}_{\boldsymbol{\theta}\boldsymbol{\alpha}} \in \mathbb{R}^{2K \times 2K}$, and $\mathbf{J}_{\boldsymbol{\alpha}\boldsymbol{\alpha}} \in \mathbb{R}^{2K \times 2K}$ are assembled from the contributions of all target pairs. Each scalar entry of the FIM is given by

$$[\mathbf{J}]_{i,j} = \frac{2}{\sigma_r^2} \Re \left\{ \sum_{\ell=1}^L \frac{\partial \boldsymbol{\mu}[\ell]^H}{\partial \xi_i} \frac{\partial \boldsymbol{\mu}[\ell]}{\partial \xi_j} \right\}, \quad i, j \in \{1, \dots, 4K\}. \quad (21)$$

Substituting the derivatives (19), which share the common structure $\frac{\partial \boldsymbol{\mu}}{\partial \xi_i} = \frac{\partial \mathbf{A}}{\partial \xi_i} \mathbf{W} \mathbf{S}$, into (21) and using $\mathbb{E}\{\mathbf{S}\mathbf{S}^H\} = \mathbf{I}$ yields

$$[\mathbf{J}]_{i,j} = \frac{2L}{\sigma_r^2} \Re \left\{ \text{tr} \left(\frac{\partial \mathbf{A}^H}{\partial \xi_i} \frac{\partial \mathbf{A}}{\partial \xi_j} \mathbf{R}_x \right) \right\}, \quad (22)$$

where $\mathbf{R}_x \triangleq \mathbf{W} \mathbf{W}^H$ is the transmit covariance matrix. This shows that the FIM, and hence the CRB, depends on \mathbf{W} only through \mathbf{R}_x .

B. Equivalence of MiLAC-aided and Digital Beamforming in Terms of CRB

The following theorem shows that, despite the restricted beamforming flexibility of lossless and reciprocal MiLAC, the MiLAC-aided and fully-digital designs achieve the same optimal CRB.

Theorem 1. *Under the assumption $M = N$ to achieve full DoFs, let $\mathcal{R}_{\text{MiLAC}} \triangleq \{\mathbf{R}_x = \mathbf{W} \mathbf{W}^H \mid \mathbf{W} \in \mathcal{W}_{\text{MiLAC}}\}$ and $\mathcal{R}_{\text{Digital}} \triangleq \{\mathbf{R}_x = \mathbf{W} \mathbf{W}^H \mid \mathbf{W} \in \mathcal{W}_{\text{Digital}}\}$ denote the sets of transmit covariance matrices achievable by MiLAC-aided and fully-digital beamforming, respectively. Then*

$$\mathcal{R}_{\text{MiLAC}} = \mathcal{R}_{\text{Digital}} = \{\mathbf{R}_x \succeq \mathbf{0} \mid \text{tr}(\mathbf{R}_x) \leq P_T\}. \quad (23)$$

¹The same $\frac{1}{2}$ factor appears in the fully-digital case, so the noise-free received signal retains the expression above with \mathbf{W} replaced by the digital beamforming matrix. The set of the digital beamforming matrix is given by $\mathcal{W}_{\text{Digital}} = \{\mathbf{W} \mid \|\mathbf{W}\|_F^2 \leq P_T\}$, which also imposes the same total transmit power constraint as the MiLAC-aided beamforming. This ensures a fair comparison between MiLAC-aided and fully-digital beamforming under the same transmit power budget.

Consequently, MiLAC-aided and fully-digital transmit beamforming designs achieve the same optimal CRB value.

Proof. We prove the two inclusions separately.

($\mathcal{R}_{\text{MiLAC}} \subseteq \mathcal{R}_{\text{Digital}}$): Since every MiLAC-achievable beamforming matrix is also digitally achievable, *i.e.*, $\mathcal{W}_{\text{MiLAC}} \subseteq \mathcal{W}_{\text{Digital}}$ [34], any transmit covariance $\mathbf{R}_x = \mathbf{W}\mathbf{W}^H$ realized by some $\mathbf{W} \in \mathcal{W}_{\text{MiLAC}}$ is also realized by the same $\mathbf{W} \in \mathcal{W}_{\text{Digital}}$.

($\mathcal{R}_{\text{Digital}} \subseteq \mathcal{R}_{\text{MiLAC}}$): Let $\mathbf{R}_x \in \mathcal{R}_{\text{Digital}}$ be an arbitrary digitally achievable transmit covariance. By definition, there exists some $\mathbf{W}' \in \mathcal{W}_{\text{Digital}}$ with $\mathbf{W}'\mathbf{W}'^H = \mathbf{R}_x$. To show $\mathbf{R}_x \in \mathcal{R}_{\text{MiLAC}}$, it suffices to find *one* $\mathbf{W} \in \mathcal{W}_{\text{MiLAC}}$ satisfying $\mathbf{W}\mathbf{W}^H = \mathbf{R}_x$. Consider the eigendecomposition $\mathbf{R}_x = \mathbf{U}\mathbf{\Lambda}\mathbf{U}^H$, where $\mathbf{U} \in \mathbb{C}^{N \times N}$ is unitary and $\mathbf{\Lambda} = \text{diag}(\lambda_1, \dots, \lambda_N) \succeq \mathbf{0}$. Construct $\mathbf{W} = \mathbf{U}\mathbf{\Lambda}^{\frac{1}{2}}$ and set $\mathbf{p} = (\lambda_1, \dots, \lambda_N)^\top$. Then: (i) $\mathbf{W}\mathbf{W}^H = \mathbf{U}\mathbf{\Lambda}\mathbf{U}^H = \mathbf{R}_x$; (ii) $\mathbf{W}^H\mathbf{W} = \mathbf{\Lambda}^{\frac{1}{2}}\mathbf{U}^H\mathbf{U}\mathbf{\Lambda}^{\frac{1}{2}} = \mathbf{\Lambda} = \text{diag}(\mathbf{p})$, so $\mathbf{W}^H\mathbf{W} \preceq \text{diag}(\mathbf{p})$; (iii) $\mathbf{1}^\top \mathbf{p} = \text{tr}(\mathbf{\Lambda}) = \text{tr}(\mathbf{R}_x) \leq P_T$. Hence $\mathbf{W} \in \mathcal{W}_{\text{MiLAC}}$ by (13), confirming $\mathbf{R}_x \in \mathcal{R}_{\text{MiLAC}}$.

Combining both inclusions yields $\mathcal{R}_{\text{MiLAC}} = \mathcal{R}_{\text{Digital}}$. Since the FIM \mathbf{J} in (20) is a function of $\mathbf{R}_x = \mathbf{W}\mathbf{W}^H$ only, the CRB $\text{tr}(\mathbf{J}^{-1})$ is identical for any two beamforming matrices sharing the same \mathbf{R}_x . The equality of the covariance sets therefore implies that MiLAC-aided and fully-digital transmit beamforming designs achieve the same optimal CRB value. ■

Remark 1. *Theorem 1 stands in contrast to the communication setting in [34], where lossless and reciprocal MiLAC-aided beamforming leads to a sum-rate loss compared to fully-digital beamforming at high SNR. The difference arises because the CRB depends on \mathbf{W} only through $\mathbf{R}_x = \mathbf{W}\mathbf{W}^H$, whereas the multiuser sum-rate depends on the individual columns of \mathbf{W} via the per-user SINR. The spectral-norm constraint $\|\mathbf{F}\|_2 \leq 1$ imposed by lossless and reciprocal MiLAC restricts the column correlations of \mathbf{W} , which excludes full-power matrices with non-orthogonal columns [34]. This restriction affects the sum-rate, which is sensitive to the column-level structure, but does not affect the CRB, which depends only on the aggregate spatial covariance \mathbf{R}_x .*

C. MiLAC Transmit Beamforming Design

We aim to design the beamforming matrix \mathbf{W} to minimize the total CRB across all target parameters and thus improve the sensing performance, subject to the MiLAC lossless and reciprocal constraints in (13). This yields the following optimization problem:

$$\mathcal{P}1 : \min_{\mathbf{W}, \mathbf{p}} \text{tr}\{\mathbf{\Xi}\} \quad (24a)$$

$$\text{s.t.} \quad \mathbf{W}^H\mathbf{W} \preceq \text{diag}(\mathbf{p}), \quad (24b)$$

$$\mathbf{1}^\top \mathbf{p} \leq P_T. \quad (24c)$$

Directly minimizing $\text{tr}\{\mathbf{\Xi}\} = \text{tr}\{\mathbf{J}^{-1}\}$ is non-convex due to the matrix inverse. Following [44], we introduce auxiliary variables $\{t_k\}_{k=1}^{4K}$ and reformulate the problem using the Schur complement. Specifically, the condition $t_k \geq [\mathbf{J}^{-1}]_{k,k}$ is equivalently expressed as the linear matrix inequality (LMI)

in (25b), where \mathbf{e}_k denotes the k th column of the $4K$ -dimensional identity matrix. Since the FIM \mathbf{J} in (20) is a linear function of the transmit covariance $\mathbf{R}_x \triangleq \mathbf{W}\mathbf{W}^H$, the resulting formulation is a semidefinite program (SDP) w.r.t. \mathbf{R}_x as follows:

$$\mathcal{P}2 : \min_{\mathbf{W}, \mathbf{p}, \{t_k\}_{k=1}^{4K}} \sum_{k=1}^{4K} \mu_k t_k \quad (25a)$$

$$\text{s.t.} \quad \begin{bmatrix} \mathbf{J} & \mathbf{e}_k \\ \mathbf{e}_k^\top & t_k \end{bmatrix} \succeq \mathbf{0}, \quad k = 1, \dots, 4K \quad (25b)$$

$$\begin{bmatrix} \mathbf{I} & \mathbf{W} \\ \mathbf{W}^H & \text{diag}(\mathbf{p}) \end{bmatrix} \succeq \mathbf{0}, \quad (25c)$$

$$\mathbf{1}^\top \mathbf{p} \leq P_T. \quad (25d)$$

The LMI constraint (25c) is transformed from the original quadratic constraint $\mathbf{W}^H\mathbf{W} \preceq \text{diag}(\mathbf{p})$ by Schur complement.

The difficulty for solving problem $\mathcal{P}2$ is that the FIM depends on \mathbf{W} through the transmit covariance $\mathbf{R}_x = \mathbf{W}\mathbf{W}^H$, whereas the MiLAC constraint involves the Gram matrix $\mathbf{W}^H\mathbf{W}$. This creates a non-trivial coupling between the two sides of \mathbf{W} . To decouple them, we introduce an auxiliary copy $\mathbf{X} = \mathbf{W}$ so that the covariance constraint $\mathbf{R}_x = \mathbf{X}\mathbf{X}^H$ is separated from the MiLAC constraint on \mathbf{W} . This leads to the following reformulation:

$$\mathcal{P}3 : \min_{\mathbf{W}, \mathbf{p}, \{t_k\}_{k=1}^{4K}} \sum_{k=1}^{4K} \mu_k t_k \quad (26a)$$

$$\text{s.t.} \quad \begin{bmatrix} \mathbf{J} & \mathbf{e}_k \\ \mathbf{e}_k^\top & t_k \end{bmatrix} \succeq \mathbf{0}, \quad k = 1, \dots, 4K \quad (26b)$$

$$\begin{bmatrix} \mathbf{I} & \mathbf{W} \\ \mathbf{W}^H & \text{diag}(\mathbf{p}) \end{bmatrix} \succeq \mathbf{0}, \quad (26c)$$

$$\mathbf{1}^\top \mathbf{p} \leq P_T, \quad (26d)$$

$$\mathbf{W} = \mathbf{X}, \quad (26e)$$

$$\mathbf{X}\mathbf{X}^H = \mathbf{R}_x. \quad (26f)$$

Problem $\mathcal{P}3$ involves two coupled constraints: the equality $\mathbf{W} = \mathbf{X}$ in (26e) and the quadratic relation $\mathbf{X}\mathbf{X}^H = \mathbf{R}_x$ in (26f). To address this problem, the penalty dual decomposition (PDD) method [40] is applied to solve (26) iteratively. Specifically, the PDD method introduces the augmented Lagrangian function by dualizing the equality constraint (26e) with a Lagrange multiplier $\mathbf{\Gamma}$ and adding a quadratic penalty term with penalty parameter $\rho > 0$. The resulting problem is:

$$\mathcal{P}4 : \min_{\mathbf{W}, \mathbf{p}, \{t_k\}_{k=1}^{4K}} \sum_{k=1}^{4K} \mu_k t_k + \frac{1}{2\rho} \|\mathbf{W} - \mathbf{X} + \rho\mathbf{\Gamma}\|^2 \quad (27a)$$

$$\text{s.t.} \quad \begin{bmatrix} \mathbf{J} & \mathbf{e}_k \\ \mathbf{e}_k^\top & t_k \end{bmatrix} \succeq \mathbf{0}, \quad k = 1, \dots, 4K \quad (27b)$$

$$\begin{bmatrix} \mathbf{I} & \mathbf{W} \\ \mathbf{W}^H & \text{diag}(\mathbf{p}) \end{bmatrix} \succeq \mathbf{0}, \quad (27c)$$

$$\mathbf{1}^\top \mathbf{p} \leq P_T, \quad (27d)$$

$$\mathbf{X}\mathbf{X}^H = \mathbf{R}_x. \quad (27e)$$

The PDD consists of an inner loop that solves the augmented Lagrangian problem and an outer loop that updates the dual variable and penalty parameter. In the inner loop, the problem is solved by alternating optimization over three variable blocks: $\{\mathbf{R}_x, \{t_k\}\}$, $\{\mathbf{W}, \mathbf{p}\}$, and \mathbf{X} . When updating each block, other variables are fixed and the designed variable is optimized by solving a convex sub-problem. In the outer loop, the dual variable $\mathbf{\Gamma}$ is updated by a gradient ascent step, and the penalty parameter ρ is updated by a geometric decay rule. This alternating optimization continues until convergence. The details of the inner loop block update and outer loop update are explained below.

1) *Inner Loop Block Update:* The details of the inner loop block update are as follows.

Update $\mathbf{R}_x, \{t_k\}_{k=1}^{4K}$. With \mathbf{W} and \mathbf{X} fixed, the penalty term in (27a) is constant, and thus the sub-problem is given by

$$\mathcal{P}5: \min_{\mathbf{R}_x, \{t_k\}_{k=1}^{4K}} \sum_{k=1}^{4K} \mu_k t_k \quad (28a)$$

$$\text{s.t.} \quad \begin{bmatrix} \mathbf{J} & \mathbf{e}_k \\ \mathbf{e}_k^\top & t_k \end{bmatrix} \succeq \mathbf{0}, k = 1, \dots, 4K \quad (28b)$$

$$\mathbf{R}_x \succeq \mathbf{0}, \quad (28c)$$

which is a SDP since the FIM \mathbf{J} is a linear function of \mathbf{R}_x , and can be solved efficiently.

Update \mathbf{p}, \mathbf{W} . With $\mathbf{R}_x, \{t_k\}$, and \mathbf{X} fixed, only the augmented Lagrangian penalty term depends on \mathbf{W} . The sub-problem w.r.t. \mathbf{W} and \mathbf{p} is given by

$$\mathcal{P}6: \min_{\mathbf{W}} \|\mathbf{W} - \mathbf{X} + \rho\mathbf{\Gamma}\|^2 \quad (29a)$$

$$\text{s.t.} \quad \begin{bmatrix} \mathbf{I} & \mathbf{W} \\ \mathbf{W}^H & \text{diag}(\mathbf{p}) \end{bmatrix} \succeq \mathbf{0}, \quad (29b)$$

$$\mathbf{1}^\top \mathbf{p} \leq P_T. \quad (29c)$$

This is also SDP and can be solved efficiently.

Update \mathbf{X} . With \mathbf{R}_x, \mathbf{W} , and \mathbf{p} fixed, the sub-problem w.r.t. \mathbf{X} aims to minimize the penalty term subject to the covariance constraint:

$$\mathcal{P}7: \min_{\mathbf{X}} \|\mathbf{X} - (\rho\mathbf{\Gamma} + \mathbf{W})\|^2 \quad (30a)$$

$$\text{s.t.} \quad \mathbf{X}\mathbf{X}^H = \mathbf{R}_x. \quad (30b)$$

To solve the sub-problem, we first define $\mathbf{\Delta} \triangleq \rho\mathbf{\Gamma} + \mathbf{W}$. Subsequently, we expand the objective function, which has the following form

$$\text{tr}(\mathbf{X}\mathbf{X}^H) - 2\Re(\text{tr}(\mathbf{\Delta}^H \mathbf{X})) + \text{tr}(\mathbf{\Delta}\mathbf{\Delta}^H). \quad (31)$$

Since the constraint fixes $\mathbf{X}\mathbf{X}^H = \mathbf{R}_x$, both $\text{tr}(\mathbf{X}\mathbf{X}^H) = \text{tr}(\mathbf{R}_x)$ and $\text{tr}(\mathbf{\Delta}\mathbf{\Delta}^H)$ are constant. The problem therefore reduces to

$$\mathcal{P}8: \min_{\mathbf{X}} \Re(\text{tr}(\mathbf{\Delta}^H \mathbf{X})) \quad (32a)$$

$$\text{s.t.} \quad \mathbf{X}\mathbf{X}^H = \mathbf{R}_x. \quad (32b)$$

Algorithm 1: Proposed Penalty-based Algorithm for MiLAC Transmit Beamforming Design

Input: $\mathbf{A}_k, k \in \mathcal{K}$, weights $\boldsymbol{\mu}$, penalty scaling factor $c \in (0, 1)$, and tolerance ϵ .

Output: $\mathbf{W}^{\text{opt}}, \mathbf{p}^{\text{opt}}$, and $\{t_k^{\text{opt}}\}_{k=1}^{4K}$.

```

1 Initialize variables  $\mathbf{W}, \mathbf{p}, \mathbf{X}, \mathbf{\Gamma} = \mathbf{0}$ ,  $\rho > 0$ , and set
   $t_{\text{out}} = 1, t_{\text{in}} = 1$ .
2 while no convergence of objective function (27a) &
   $\|\mathbf{W} - \mathbf{X}\|_\infty > \epsilon$  &  $t_{\text{out}} < t_{\text{max}}^{\text{out}}$  do
3   while no convergence of objective function (27a)
    &  $t_{\text{in}} < t_{\text{max}}^{\text{in}}$  do
4     Update  $\mathbf{R}_x$  and  $\{t_k\}_{k=1}^{4K}$  by solving the
      subproblem (28).
5     Update  $\mathbf{p}$  and  $\mathbf{W}$  by solving the subproblem
      (29).
6     Update auxiliary variable  $\mathbf{X}$  by (35),
      i.e.,  $\mathbf{X} = \mathbf{R}_x^{1/2} \mathbf{U} \mathbf{V}^H$ .
7      $t_{\text{in}} = t_{\text{in}} + 1$ .
8   end
9   if  $\|\mathbf{W} - \mathbf{X}\|_\infty < \epsilon$  then
10    Update the dual variable  $\mathbf{\Gamma}$  via
       $\mathbf{\Gamma} = \mathbf{\Gamma} + \rho^{-1}(\mathbf{W} - \mathbf{X})$ .
11   end
12   else
13    Update the penalty coefficient  $\rho$  via  $\rho = c\rho$ .
14   end
15    $t_{\text{out}} = t_{\text{out}} + 1$ .
16 end
17 Return  $\mathbf{W}^{\text{opt}}, \mathbf{p}^{\text{opt}}$  and  $\{t_k^{\text{opt}}\}_{k=1}^{4K}$ .

```

Substituting $\mathbf{X} = \mathbf{R}_x^{1/2} \mathbf{Q}$ with $\mathbf{Q}\mathbf{Q}^H = \mathbf{I}$, which automatically satisfies the constraint $\mathbf{X}\mathbf{X}^H = \mathbf{R}_x$, the problem becomes the unitary Procrustes problem [45]:

$$\mathcal{P}9: \min_{\mathbf{Q}} \Re(\text{tr}(\mathbf{\Psi}^H \mathbf{Q})), \quad (33a)$$

$$\text{s.t.} \quad \mathbf{Q}\mathbf{Q}^H = \mathbf{I}, \quad (33b)$$

where $\mathbf{\Psi} \triangleq \mathbf{R}_x^{1/2} \mathbf{\Delta}$. Let $\mathbf{\Psi} = \mathbf{U}\mathbf{\Sigma}\mathbf{V}^H$ be its singular value decomposition (SVD). The closed-form solution is [45]

$$\mathbf{Q} = \mathbf{U}\mathbf{V}^H. \quad (34)$$

The original variable \mathbf{X} is then recovered as

$$\mathbf{X} = \mathbf{R}_x^{1/2} \mathbf{Q} = \mathbf{R}_x^{1/2} \mathbf{U}\mathbf{V}^H. \quad (35)$$

2) *Outer Loop:* Once the inner loop converges, the outer loop checks whether the equality constraint $\mathbf{W} = \mathbf{X}$ is sufficiently satisfied, using the criterion $\|\mathbf{W} - \mathbf{X}\|_\infty < \epsilon$ for a small positive threshold ϵ . If the criterion is met, the dual variable is updated as

$$\mathbf{\Gamma} = \mathbf{\Gamma} + \rho^{-1}(\mathbf{W} - \mathbf{X}). \quad (36)$$

Otherwise, the penalty coefficient is tightened via $\rho = c\rho$, $c \in (0, 1)$, to strengthen the enforcement of the equality constraint in subsequent iterations. The overall procedure is summarized in Algorithm 1.

Algorithm 2: SDP-based Algorithm for Digital Transmit Beamforming Design

Input: $\mathbf{A}_k, k \in \mathcal{K}$.

Output: \mathbf{W}^{opt} , and $\{t_k^{\text{opt}}\}_{k=1}^{4K}$.

- 1 Initialize variables \mathbf{R}_x .
 - 2 Update \mathbf{R}_x and $\{t_k\}_{k=1}^{4K}$ by solving the convex problem (38).
 - 3 Reconstruct \mathbf{W} from \mathbf{R}_x .
 - 4 Return \mathbf{W}^{opt} and $\{t_k^{\text{opt}}\}_{k=1}^{4K}$.
-

D. Digital Beamforming Design

We also provide the digital beamforming design as a performance benchmark. In the digital beamforming architecture, the transmit beamformer $\mathbf{W} \in \mathbb{C}^{N \times M}$ is fully digital with only the power constraint $\|\mathbf{W}\|_F^2 \leq P_T$. The CRB minimization problem is formulated as

$$\mathcal{P}10 : \min_{\mathbf{W}} \quad \text{tr}\{\mathbf{\Xi}\} \quad (37a)$$

$$\text{s.t.} \quad \|\mathbf{W}\|_F^2 \leq P_T. \quad (37b)$$

This problem can be transformed by SDP and letting $\mathbf{R}_x = \mathbf{W}\mathbf{W}^H \in \mathbb{C}^{N \times N}$, which is given by

$$\mathcal{P}11 : \min_{\mathbf{R}_x, \{t_k\}_{k=1}^{4K}} \quad \sum_{k=1}^{4K} \mu_k t_k \quad (38a)$$

$$\text{s.t.} \quad \begin{bmatrix} \mathbf{J} & \mathbf{e}_k \\ \mathbf{e}_k^\top & t_k \end{bmatrix} \succeq \mathbf{0}, \quad k = 1, \dots, 4K \quad (38b)$$

$$\text{tr}(\mathbf{R}_x) \leq P_T, \quad (38c)$$

$$\mathbf{R}_x \succeq \mathbf{0}. \quad (38d)$$

Since this problem is SDP, it can be solved efficiently as summarized in Algorithm 2. Subsequently, \mathbf{W} is reconstructed from \mathbf{R}_x .

Compared to the MiLAC design in Algorithm 1, the digital beamforming design is simpler because the CRB depends on \mathbf{W} only through the transmit covariance $\mathbf{R}_x = \mathbf{W}\mathbf{W}^H$, so the optimization reduces to an SDP in \mathbf{R}_x . However, in the MiLAC case, the lossless-reciprocal constraint $\mathbf{W}^H\mathbf{W} \preceq \text{diag}(\mathbf{p})$ couples \mathbf{W} on both sides of the inequality. This prevents a direct reformulation in terms of \mathbf{R}_x . This structural difficulty thus motivates the proposed PDD-based algorithm.

E. Convergence Analysis

We briefly analyze the convergence of Algorithm 1 and show that at least a local optimum of the problem $\mathcal{P}4$ can be obtained. We first denote value of objective function (27a) at iteration t as f^t . In the inner loop of Algorithm 1, the three subproblems $\mathcal{P}5$, $\mathcal{P}6$, and $\mathcal{P}7$ are both convex and thus can be solved to global optimality, ensuring that f^t is non-increasing and a Karush–Kuhn–Tucker (KKT) point of the inner problem $\mathcal{P}4$ can be achieved at convergence. In the outer loop, the penalty coefficient ρ is adaptively updated to enforce the equality constraint $\mathbf{W} = \mathbf{X}$. According to [40], Theorem

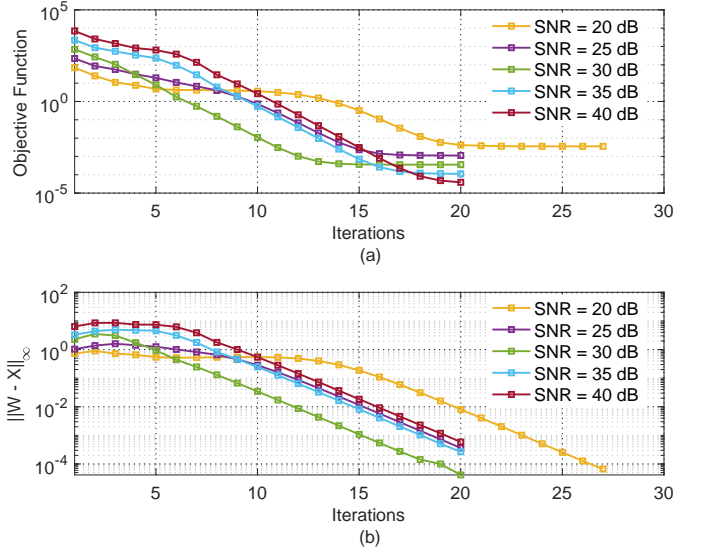


Fig. 4. Convergence of Algorithm 1 with $N = 64$ transmit antennas and 2 targets for detection. (a) Value of objective function (27a) versus iteration numbers. (b) Difference between \mathbf{W} and auxiliary variable \mathbf{X} .

3.1], the proposed PDD algorithm converges to a KKT point of $\mathcal{P}4$ with $\epsilon \rightarrow 0$.

We evaluate the convergence behavior of Algorithm 1 through numerical simulations. Specifically, we check the convergence of the objective function value (27a) in Fig. 4 (a) and the primal residual $\|\mathbf{W} - \mathbf{X}\|_\infty$ in Fig. 4 (b) versus iterations. The simulation parameters are set as $N = 8 \times 8 = 64$ transmit antennas and $K = 2$ targets. With different SNRs, the objective function value decreases monotonically and converges in 30 iterations, as shown in Fig. 4(a). The curve with a higher SNR converges to a lower objective value, which is consistent with the fact that a higher SNR leads to a lower CRB. In addition, the primal residual $\|\mathbf{W} - \mathbf{X}\|_\infty$ decreases monotonically and falls below the tolerance $\epsilon = 10^{-3}$ in 30 iterations, demonstrating the effectiveness of algorithm to enforce the equality constraint $\mathbf{W} = \mathbf{X}$.

F. Complexity Analysis

We analyze the per-iteration complexity of Algorithm 1 with $M = N$. Using the standard interior-point SDP complexity $\mathcal{O}(n^2 p^{2.5} + p^{3.5})$ for n variables and LMI constraints of size p , the sub-problem $\mathcal{P}7$ dominates the computational complexity due to its $(N + M)$ -size LMI constraint, which yields a per-iteration complexity of $\mathcal{O}(N^{6.5})$. Therefore, the overall complexity of Algorithm 1 is given by $\mathcal{O}(I_{\text{out}} I_{\text{in}} N^{6.5})$, where I_{out} and I_{in} denote the maximum numbers of outer and inner iterations of the PDD method, respectively.

IV. RECEIVER-SIDE MiLAC DESIGN FOR DOA ESTIMATION

In this section, we design the receiver-side MiLAC to implement the 2D DFT for analog-domain DoA estimation. We first formulate the optimization problem and derive a closed-form solution. Then, we take the snapshots into account and extend the design to implement the fractional 2D DFT for improved DoA estimation performance.

A. Problem Formulation and Closed-form Solution

The target angles are estimated by applying the 2D DFT to the received signal in (14) and locating the spectral peaks. The (n, n') th element of the normalized 2D DFT matrix $\mathbf{F}_{\text{DFT}} \in \mathbb{C}^{N \times N}$ is given by [46]

$$f_{n,n'} = \frac{1}{\sqrt{N}} e^{-j2\pi \frac{(n_x-1)(n'_x-1)}{N_x}} e^{-j2\pi \frac{(n_y-1)(n'_y-1)}{N_y}}, \quad (39)$$

where n_x and n_y are defined in (6). Our goal is to design $\mathbf{V}_{\text{MiLAC}}$ within the feasible set (15) so that it approximates \mathbf{F}_{DFT} , therefore enabling analog-domain DoA estimation without high-complexity digital processing.

We measure the approximation quality by the Frobenius-norm error

$$\mathcal{L} = \|\beta \mathbf{V}_{\text{MiLAC}} - \mathbf{F}_{\text{DFT}}\|_F^2, \quad (40)$$

where β is a scaling factor for normalization. The optimization problem is

$$\mathcal{P}12: \min_{\mathbf{V}_{\text{MiLAC}}} \mathcal{L} = \|\beta \mathbf{V}_{\text{MiLAC}} - \mathbf{F}_{\text{DFT}}\|_F^2 \quad (41a)$$

$$\text{s.t.} \quad \mathbf{V}_{\text{MiLAC}} = \frac{1}{2} [\Theta]_{N+1:2N, 1:N}, \quad (41b)$$

$$\Theta = \Theta^\top, \quad (41c)$$

$$\Theta^H \Theta = \mathbf{I}. \quad (41d)$$

Since \mathbf{F}_{DFT} is unitary, *i.e.*, $\mathbf{F}_{\text{DFT}}^H \mathbf{F}_{\text{DFT}} = \mathbf{I}$, the global optimum is obtained at $\mathbf{V}_{\text{MiLAC}} = \frac{1}{2} \mathbf{F}_{\text{DFT}}$ and $\beta = 2$ with zero approximation error. Substituting this into (9), the corresponding scattering matrix is

$$\Theta = \begin{bmatrix} \mathbf{0} & \mathbf{F}_{\text{DFT}}^\top \\ \mathbf{F}_{\text{DFT}} & \mathbf{0} \end{bmatrix}. \quad (42)$$

This closed-form solution shows that the receiver-side MiLAC can implement the 2D DFT exactly, without any offline iterative optimization.

B. Fractional 2D DFT for DoA Estimation

To improve the DoA estimation performance, we can leverage the snapshots across time slots to implement a fractional 2D DFT, which provides finer spatial-frequency resolution than the standard 2D DFT. Specifically, this approach generates a set of orthogonal spatial-frequency bins by reconfiguring the receive-side MiLAC at each time slot ℓ to implement the fractional 2D DFT matrix as in (43). The L snapshots are divided into L_y blocks, each of length L_x , such that $L = L_x L_y$. The normalized fractional 2D DFT matrix at time slot ℓ is given by [27], [46]

$$f_{n,n',\ell} = \frac{1}{\sqrt{N}} e^{-j2\pi \frac{(n_x-1)(n'_x-1 + \frac{\ell_x-1}{L_x})}{N_x}} e^{-j2\pi \frac{(n_y-1)(n'_y-1 + \frac{\ell_y-1}{L_y})}{N_y}}, \quad (43)$$

where n_x and n_y are the physical antenna indices defined in (6). The block index ℓ_y and the time-slot index ℓ_x within that block are defined by

$$\ell_y = \lceil \ell / L_x \rceil, \quad \ell_x = \ell - (\ell_y - 1) L_x. \quad (44)$$

Subsequently, at each time slot ℓ , the MiLAC is reconfigured to implement the fractional 2D DFT matrix by solving the

optimization problem in (41) with \mathbf{F}_{DFT} replaced by $\mathbf{F}_{\text{DFT},\ell}$ with each element given by (43). The MiLAC-processed signal \mathbf{Z} in (14) is then evaluated over the joint spatial-time domain to identify the K dominant peaks corresponding to the K targets. For the k th target, the peak pair $(\hat{n}_k, \hat{\ell}_k)$ is

$$(\hat{n}_k, \hat{\ell}_k) = \arg \max_{\substack{n \in \{1, \dots, N\} \\ \ell \in \{1, \dots, L\} \\ (n, \ell) \notin \hat{\mathcal{I}}_{k-1}}} |z_{n,\ell}|^2, \quad \text{for } k = 1, \dots, K, \quad (45)$$

where $\hat{\mathcal{I}}_{k-1} = \{(\hat{n}_1, \hat{\ell}_1), \dots, (\hat{n}_{k-1}, \hat{\ell}_{k-1})\}$ is the set of previously identified peak indices, with $\hat{\mathcal{I}}_0 = \emptyset$. The corresponding electrical angles for the k th target are then obtained as

$$\begin{aligned} \hat{\psi}_{x,k} &= \text{mod} \left(2 \left(\frac{\hat{n}_{x,k} - 1}{N_x} + \frac{\hat{\ell}_{x,k} - 1}{N_x L_x} \right) + 1, 2 \right) - 1, \\ \hat{\psi}_{y,k} &= \text{mod} \left(2 \left(\frac{\hat{n}_{y,k} - 1}{N_y} + \frac{\hat{\ell}_{y,k} - 1}{N_y L_y} \right) + 1, 2 \right) - 1, \end{aligned} \quad (46)$$

where $\hat{n}_{x,k}$ and $\hat{n}_{y,k}$ are obtained by substituting \hat{n}_k into (6), while $\hat{\ell}_{x,k}$ and $\hat{\ell}_{y,k}$ are obtained by substituting $\hat{\ell}_k$ into (44). Finally, the azimuth and elevation estimates follow from inverting (1) as

$$\hat{\varphi}_k = \arctan \left(\frac{\hat{\psi}_{y,k} d_x}{\hat{\psi}_{x,k} d_y} \right), \quad \hat{\vartheta}_k = \arcsin \left(\frac{1}{\kappa} \sqrt{\frac{\hat{\psi}_{x,k}^2}{d_x^2} + \frac{\hat{\psi}_{y,k}^2}{d_y^2}} \right). \quad (47)$$

This MiLAC-aided fractional 2D DFT approach removes the RF chains and ADCs at the receiver due to the received RF signals are directly processed in the analog domain, which significantly reduces the hardware cost and power consumption. In contrast, the conventional radar system requires N RF chains and ADCs to down-convert and digitize the received signal for DoA estimation.

V. NUMERICAL EVALUATION

In this section, we evaluate the performance of the proposed MiLAC-aided MIMO radar sensing system. The system employs a co-located UPA with half-wavelength element spacing, *i.e.*, $d_x = d_y = \lambda/2$. The UPA is assumed to be square with $N_x = N_y$ and hence $N = N_x \times N_y$. The noise power is normalized to $\sigma_r^2 = 1$, and the total receive radar SNR is defined as $\text{SNR} = 10 \log_{10} \left(\sum_{k=1}^K \alpha_{r,k}^2 P_T / \sigma_r^2 \right)$, where P_T is the total transmit power. To improve the DoA estimation performance, we consider L snapshot observations at the receiver using a fractional DFT-based approach as explained in Section IV-B. The penalty scaling factor and convergence tolerance are set as $c = 0.5$ and $\epsilon = 10^{-3}$, respectively. Three baseline schemes are considered for comparison: on the transmit side, (i) the *digital beamforming design* (Algorithm 2), which serves as a performance lower bound on the CRB, and (ii) the *matched filter*, which steers the transmit beam toward the target directions using the steering vectors; on the receive side, (iii) the *digital 2D DFT-based DoA estimator*, which performs the 2D DFT computation digitally.

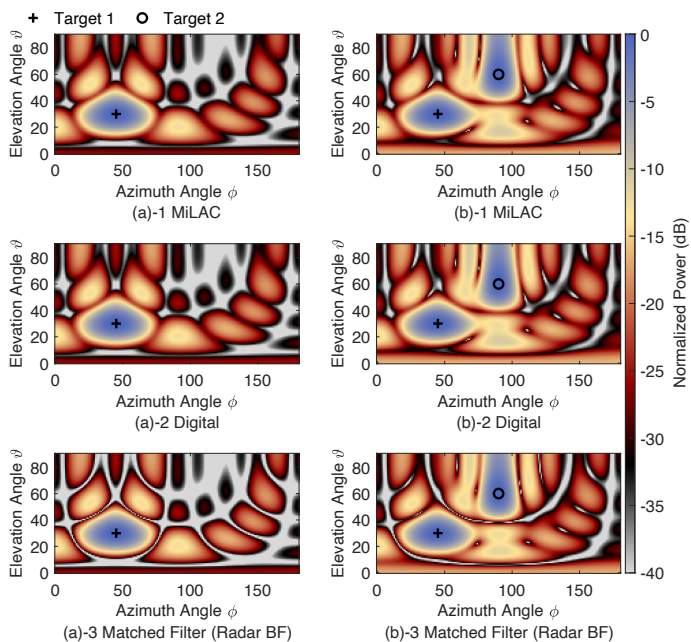


Fig. 5. Transmit beampattern with $N = 64$ transmit antennas with receive radar SNR = 20 dB. The optimized beampatterns with 1 target are shown in (a)-1 MiLAC , (a)-2 digital and (a)-3 matched filter beamforming design. The optimized beampatterns with 2 targets are shown in (b)-1 MiLAC , (b)-2 digital and (b)-3 matched filter beamforming design.

A. MiLAC-aided Transmit Beamforming Design

1) *Beampattern Performances*: Fig. 5 compares the 2D transmit beampatterns generated by three kinds of beamforming designs with $N = 64$ antennas with 20 dB SNR. For the single-target case ($K = 1$), Fig. 5(a)-1 shows the MiLAC design, Fig. 5(a)-2 shows the fully-digital design, and Fig. 5(a)-3 shows the matched filter design. In addition, we also plot the beampattern when two targets are present from Fig. 5(b)-1 to (b)-3. It can be observed that: (i) the MiLAC-aided beamforming design can probe to the correct target directions. In comparison to the matched filter, the MiLAC design can generate a sharper main lobe and lower side lobes, which is beneficial for improving the estimation performance. (ii) The beampattern of the MiLAC design has the same performance to the fully-digital design. This demonstrates that constraints imposed by MiLAC do not degrade the beamforming capability relative to the fully-digital design.

2) *CRB Performances*: To quantitatively evaluate the estimation performance, we compute the CRB using the FIM derived in (20) with the optimal beamformers obtained from Algorithm 1 and Algorithm 2, respectively, and compare the proposed MiLAC-aided design against the fully-digital benchmark.

We first evaluate the CRB versus the receive radar SNR with $K = 3$ targets and $N = 16$ antennas. The targets are located at $(\varphi, \vartheta) = (30^\circ, 30^\circ), (60^\circ, 45^\circ),$ and $(90^\circ, 60^\circ)$. As shown in Fig. 6, the CRB decreases with increasing SNR for both schemes, and the MiLAC design achieves CRB performance the same as the fully-digital design across the entire SNR range.

Fig. 7 plots the CRB versus the number of targets K with

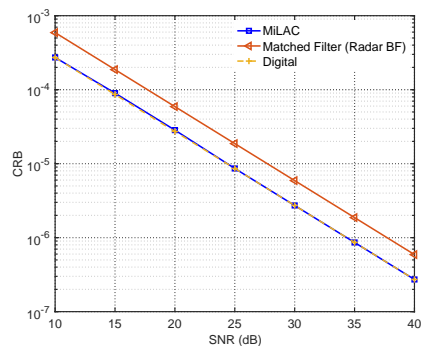


Fig. 6. CRB of 3 target versus receive radar SNR with number of antennas $N = 16$. The targets are located at $(\varphi, \vartheta) = (30^\circ, 30^\circ), (60^\circ, 45^\circ),$ and $(90^\circ, 60^\circ)$.

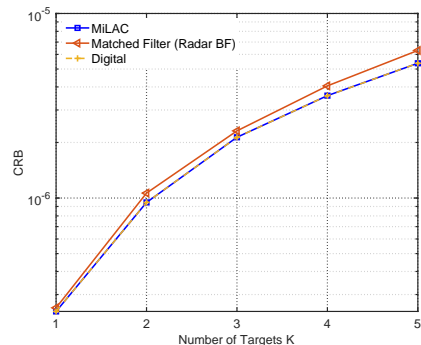


Fig. 7. CRB versus number of targets with number of antennas $N = 64$ and receive radar SNR 20 dB.

$N = 64$ antennas and a fixed SNR of 20 dB. As the number of targets increases, the CRB increases for both designs because more unknown parameters need to be estimated and the transmit power per target is reduced. The MiLAC design consistently achieves CRB performance the same to the fully-digital benchmark.

Across all evaluations, the proposed MiLAC-aided design obtains same CRB performances as the fully-digital benchmark regardless of the SNR, and number of targets. This verifies the theoretical analysis that the MiLAC-aided beamforming design can achieve the same CRB as the fully-digital design in Section III-B.

B. MiLAC-aided Receiver Side DoA Estimator

1) *Computational Complexity*: The complexity of 1D DFT in the column and row are $34/9N_y \log_2(N_y)$ and $34/9N_x \log_2(N_x)$, respectively [47], thus the total complexity of 2D DFT is $34/9N \log_2(N)$. Here, $N = N_x N_y$, and we assume $N_x = N_y$ for simplicity so that the UPA is square. Since we consider the fractional 2D DFT with L snapshots, the total complexity of the digital 2D DFT is $34/9LN \log_2(N)$. In contrast, the MiLAC-aided 2D DFT is generated instantly in the analog domain requiring no digital operations [29]. Therefore, the computational complexity of the MiLAC-aided 2D DFT is significantly lower than the digital 2D DFT. Fig. 8 illustrates the computational complexity of both approaches versus the number of antennas N with $L = 2500$. The MiLAC-aided approach maintains a constant

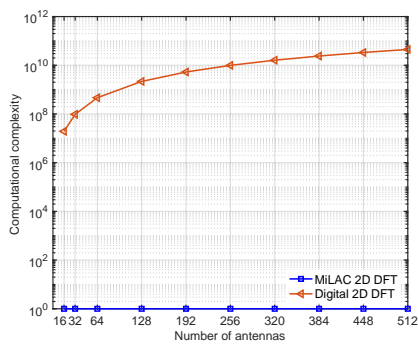


Fig. 8. Computational complexity of digital and MiLAC 2D DFT with $L = 2500$.

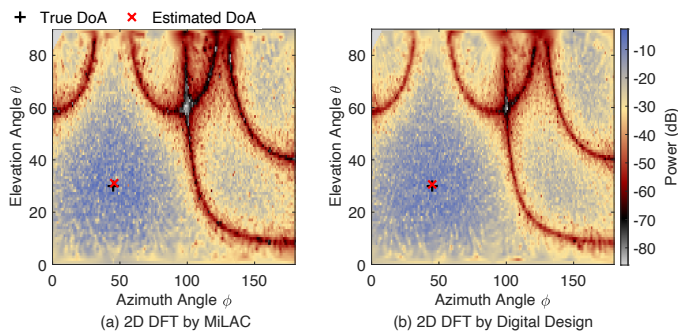


Fig. 9. Angular spectrum of the received signal with 1 target. The physical angles of the target are $(\vartheta, \varphi) = (45^\circ, 30^\circ)$. Parameters: SNR = 20 dB, $N = 16$ antennas, and $L = 2500$ snapshots.

complexity regardless of N . The benefit of lower complexity of MiLAC becomes more significant as the number of antennas and snapshots increases, this is particularly advantageous for massive MIMO radar systems.

2) *Detection results:* In this part, we evaluate the DoA estimation performance of the MiLAC-aided receiver, which performs the 2D DFT in the analog domain via the MiLAC (42). Fig. 9 (a) shows the angular spectrum obtained from the MiLAC-aided receiver for a single target located at $(\vartheta, \varphi) = (45^\circ, 30^\circ)$ with $N = 4 \times 4 = 16$ antennas and $L = 2500$ snapshots with 20 dB SNR. The spectrum shows a peak at the true target location. Compared to Fig. 9 (b) which is the fully-digital approach, this confirms that the MiLAC successfully implements the 2D DFT and enables accurate DoA detection without digital processing.

We extend the detection to the multi-target case with targets at $(\vartheta, \varphi) = (45^\circ, 30^\circ)$ and $(90^\circ, 60^\circ)$, using $N = 64$ antennas and $L = 400$ snapshots. Both targets are clearly detected in the angular spectrum. This demonstrates the ability of the MiLAC-aided receiver to detect multiple targets. In addition, the larger antenna array has finer angular resolution.

3) *MSE Performances of Parameter Estimation:* Finally, we compare the mean squared error (MSE) of the DoA estimation between the MiLAC-aided approach and the fully-digital 2D DFT-based method. The “MiLAC” label refers to utilizing the MiLAC-aided transmit beamforming (Algorithm 1) combined with MiLAC-aided analog 2D DFT reception. “Digital” refers to the digital transmit beamforming design (Algorithm 2) combined with digital 2D DFT processing.

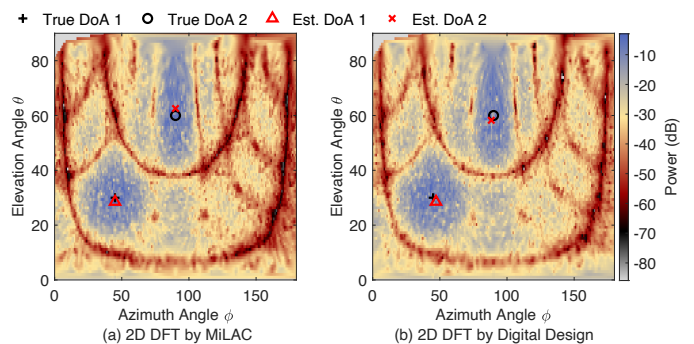


Fig. 10. Angular spectrum of the received signal with 2 targets. The physical angles are $(\vartheta, \varphi) = (45^\circ, 30^\circ)$ and $(90^\circ, 60^\circ)$, respectively. Parameters: SNR = 20 dB, $N = 64$ antennas, and $L = 400$ snapshots.

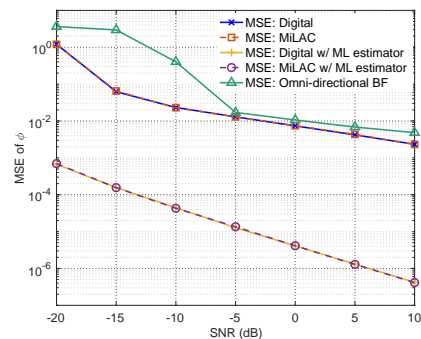


Fig. 11. MSE comparison of single-target DoA estimation versus θ for the MiLAC-aided and conventional 2D digital DFT-based methods, with $N = 16$ antennas and $T = 256$ snapshots. “MiLAC” denotes MiLAC-aided transmit beamforming and DoA estimation, while “Digital” denotes digital transmit beamforming and digital 2D DFT.

We take the estimation of the azimuth angle φ as examples. In Fig. 11, it shows the MSE versus SNR of the estimated azimuth angle φ for a single target, where $N = 16$ antennas and $T = 256$ snapshots. The MiLAC-aided estimator achieves MSE performance comparable to the fully-digital approach across all SNRs. In addition, the MSE is lower bounded by the maximum likelihood (ML) estimator. Specifically, the bound is obtained by adopting the ML estimator with both MiLAC-aided and digital transmit beamforming as shown in Fig. 11. We subsequently increase the number of antennas to $N = 64$ and the number of snapshots to $T = 4096$. Fig. 12 illustrates that the MiLAC-aided method has the same performance as the fully-digital method. Additionally, due to the larger array aperture and more snapshots, the MSE is reduced compared to the $N = 16$ case. The 2D DFT-based DoA estimator cannot reach the bound of the ML estimator is due to that the DFT-based estimator is a sub-optimal estimator, and the estimation error is affected by the grid mismatch between the true target angles and the DFT bins. The MSE can be reduced by increasing the number of antennas and snapshots as shown in Fig. 11 and Fig. 12 or adopting off-grid estimation methods [48]. These results confirm that the MiLAC-aided approach achieves the same estimation accuracy compared to the fully-digital system with significantly reduced hardware cost and computational complexity.

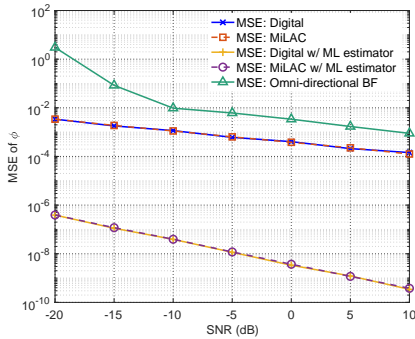


Fig. 12. MSE comparison of single-target DoA estimation versus θ for the MiLAC-aided and conventional 2D digital DFT-based methods, with $N = 64$ antennas and $T = 4096$ snapshots.

VI. CONCLUSION

In this paper, we have proposed a MiLAC-aided MIMO radar sensing approach that implements both transmit beamforming and receiver-side 2D-DFT-based DoA estimation. On the transmit side, we have formulated the beamforming design as a weighted CRB minimization problem subject to the total transmit power constraint and the lossless and reciprocal constraints imposed by the MiLAC, and developed a PDD-based iterative algorithm to solve the resulting non-convex problem. We have further proved that MiLAC-aided and fully-digital beamforming achieve the same optimal CRB, because the CRB depends on the beamforming matrix only through the transmit covariance and the set of achievable transmit covariance matrices is identical under both architectures. On the receiver side, we have shown that the 2D DFT can be exactly implemented by a lossless reciprocal MiLAC in closed form, enabling analog-domain DoA estimation. Numerical results have confirmed the theoretical finding and demonstrated that MiLAC-aided DoA estimation achieves MSE performance the same as the fully-digital benchmark, while significantly reducing hardware cost and computational complexity. These results confirm that MiLAC is a promising hardware architecture for MIMO radar sensing, which reduces hardware cost and power consumption due to employing low-resolution DACs at the transmitter and eliminating RF chains and ADCs at the receiver, as well as eliminates all digital DFT operations for DoA estimation. Future work will explore designing MiLAC to support high-resolution DoA estimation algorithms such as MUSIC.

APPENDIX A: DERIVATION OF THE FISHER INFORMATION MATRICES

In this appendix, we derive the angle-dependent derivatives of the round-trip steering matrix used in the FIM construction. Recall that $\mathbf{A}(\psi_x, \psi_y) = \mathbf{b}(\psi_x, \psi_y)\mathbf{a}^\top(\psi_x, \psi_y) \in \mathbb{C}^{N \times N}$. Since \mathbf{A} depends on the electrical angles ψ_x and ψ_y , and these electrical angles are in turn functions of the physical angles ϑ and φ , the chain rule gives

$$\frac{\partial \mathbf{A}}{\partial \vartheta} = \frac{\partial \mathbf{A}}{\partial \psi_x} \frac{\partial \psi_x}{\partial \vartheta} + \frac{\partial \mathbf{A}}{\partial \psi_y} \frac{\partial \psi_y}{\partial \vartheta}, \quad (48)$$

$$\frac{\partial \mathbf{A}}{\partial \varphi} = \frac{\partial \mathbf{A}}{\partial \psi_x} \frac{\partial \psi_x}{\partial \varphi} + \frac{\partial \mathbf{A}}{\partial \psi_y} \frac{\partial \psi_y}{\partial \varphi}. \quad (49)$$

We therefore first derive $\frac{\partial \mathbf{A}}{\partial \psi_x}$ and $\frac{\partial \mathbf{A}}{\partial \psi_y}$. Using the product rule, we obtain

$$\dot{\mathbf{A}}_{\psi_x}(\psi_x, \psi_y) = \frac{\partial \mathbf{A}}{\partial \psi_x} = \frac{\partial \mathbf{b}}{\partial \psi_x} \mathbf{a}^\top + \mathbf{b} \frac{\partial \mathbf{a}^\top}{\partial \psi_x}. \quad (50)$$

To simplify the derivation, define $\mathbf{D}_x = \text{diag}(0, 1, 2, \dots, N_x - 1)$ and $\mathbf{D}_y = \text{diag}(0, 1, 2, \dots, N_y - 1)$. The derivatives of the one-dimensional steering vectors are then given by

$$\frac{\partial \mathbf{a}_x(\psi_x)}{\partial \psi_x} = j\mathbf{D}_x \mathbf{a}_x(\psi_x). \quad (51)$$

$$\frac{\partial \mathbf{a}_y(\psi_y)}{\partial \psi_y} = j\mathbf{D}_y \mathbf{a}_y(\psi_y) \quad (52)$$

Substituting these expressions into the Kronecker-product steering-vector model yields

$$\begin{aligned} \frac{\partial \mathbf{a}}{\partial \psi_x} &= \mathbf{a}_y(\psi_y) \otimes \left(\frac{\partial \mathbf{a}_x(\psi_x)}{\partial \psi_x} \right) = \mathbf{a}_y(\psi_y) \otimes (j\mathbf{D}_x \mathbf{a}_x(\psi_x)) \\ &= j(\mathbf{I} \otimes \mathbf{D}_x) \mathbf{a}(\psi_x, \psi_y) \end{aligned} \quad (53)$$

$$\begin{aligned} \frac{\partial \mathbf{a}}{\partial \psi_y} &= \left(\frac{\partial \mathbf{a}_y(\psi_y)}{\partial \psi_y} \right) \otimes \mathbf{a}_x(\psi_x) = (j\mathbf{D}_y \mathbf{a}_y(\psi_y)) \otimes \mathbf{a}_x(\psi_x) \\ &= j(\mathbf{D}_y \otimes \mathbf{I}) \mathbf{a}(\psi_x, \psi_y) \end{aligned} \quad (54)$$

For notational convenience, define $\mathbf{D}_{\psi_x} = j(\mathbf{I} \otimes \mathbf{D}_x)$ and $\mathbf{D}_{\psi_y} = j(\mathbf{D}_y \otimes \mathbf{I})$. Then

$$\frac{\partial \mathbf{A}}{\partial \psi_x} = (\mathbf{D}_{\psi_x} \mathbf{b}) \mathbf{a}^\top + \mathbf{b} (\mathbf{D}_{\psi_x} \mathbf{a})^\top. \quad (55)$$

Since $\mathbf{D}_{\psi_x}^\top = \mathbf{D}_{\psi_x}$, this expression simplifies to

$$\frac{\partial \mathbf{A}}{\partial \psi_x} = \mathbf{D}_{\psi_x} \mathbf{A} + \mathbf{A} \mathbf{D}_{\psi_x}. \quad (56)$$

Applying the same argument to the y -direction gives

$$\frac{\partial \mathbf{A}}{\partial \psi_y} = (\mathbf{D}_{\psi_y} \mathbf{b}) \mathbf{a}^\top + \mathbf{b} (\mathbf{D}_{\psi_y} \mathbf{a})^\top = \mathbf{D}_{\psi_y} \mathbf{A} + \mathbf{A} \mathbf{D}_{\psi_y}. \quad (57)$$

We next relate the electrical-angle derivatives to the physical-angle derivatives. From (1), we have

$$\frac{\partial \psi_x}{\partial \vartheta} = \kappa d_x \cos(\vartheta) \cos(\varphi), \quad \frac{\partial \psi_y}{\partial \vartheta} = \kappa d_y \cos(\vartheta) \sin(\varphi), \quad (58)$$

$$\frac{\partial \psi_x}{\partial \varphi} = -\kappa d_x \sin(\vartheta) \sin(\varphi), \quad \frac{\partial \psi_y}{\partial \varphi} = \kappa d_y \sin(\vartheta) \cos(\varphi). \quad (59)$$

Substituting these derivatives into the chain-rule expressions at the beginning of the appendix yields

$$\frac{\partial \mathbf{A}}{\partial \vartheta} = [\kappa d_x \cos(\vartheta) \cos(\varphi)] \frac{\partial \mathbf{A}}{\partial \psi_x} + [\kappa d_y \cos(\vartheta) \sin(\varphi)] \frac{\partial \mathbf{A}}{\partial \psi_y}, \quad (60)$$

$$\frac{\partial \mathbf{A}}{\partial \varphi} = [-\kappa d_x \sin(\vartheta) \sin(\varphi)] \frac{\partial \mathbf{A}}{\partial \psi_x} + [\kappa d_y \sin(\vartheta) \cos(\varphi)] \frac{\partial \mathbf{A}}{\partial \psi_y}. \quad (61)$$

REFERENCES

- [1] N. González-Prelcic, M. F. Keskin, O. Kaltiokallio, M. Valkama, D. Dardari, X. Shen, Y. Shen, M. Bayraktar, and H. Wymeersch, "The integrated sensing and communication revolution for 6G: Vision, techniques, and applications," *Proc. IEEE*, vol. 112, no. 7, pp. 676–723, 2024.
- [2] J. Li and P. Stoica, "MIMO radar with colocated antennas," *IEEE Signal Process. Mag.*, vol. 24, no. 5, pp. 106–114, 2007.
- [3] P. Stoica, J. Li, and Y. Xie, "On probing signal design for MIMO radar," *IEEE Trans. Sig. Proc.*, vol. 55, no. 8, pp. 4151–4161, 2007.
- [4] D. R. Fuhrmann and G. San Antonio, "Transmit beamforming for MIMO radar systems using signal cross-correlation," *IEEE Trans. Aerosp. Electron. Syst.*, vol. 44, no. 1, pp. 171–186, 2008.
- [5] A. Hassanien, S. A. Vorobyov, and A. B. Gershman, "Moving target parameters estimation in noncoherent MIMO radar systems," *IEEE Trans. Sig. Proc.*, vol. 60, no. 5, pp. 2354–2361, 2012.
- [6] B. Tang, M. M. Naghsh, and J. Tang, "Relative entropy-based waveform design for MIMO radar detection in the presence of clutter and interference," *IEEE Trans. Sig. Proc.*, vol. 63, no. 14, pp. 3783–3796, 2015.
- [7] S. Sun, A. P. Petropulu, and H. V. Poor, "MIMO radar for advanced driver-assistance systems and autonomous driving: Advantages and challenges," *IEEE Signal Process. Mag.*, vol. 37, no. 4, pp. 98–117, 2020.
- [8] D. Tarchi, F. Oliveri, and P. F. Sarmartino, "MIMO radar and ground-based SAR imaging systems: Equivalent approaches for remote sensing," *IEEE Trans. Geosci. Remote Sens.*, vol. 51, no. 1, pp. 425–435, 2012.
- [9] Z. Liu, S. Aditya, H. Li, and B. Clerckx, "Joint transmit and receive beamforming design in full-duplex integrated sensing and communications," *IEEE J. Sel. Areas Commun.*, vol. 41, no. 9, pp. 2907–2919, 2023.
- [10] E. Björnson, L. Sanguinetti, H. Wymeersch, J. Hoydis, and T. L. Marzetta, "Massive MIMO is a reality—what is next?: Five promising research directions for antenna arrays," *Digital Signal Processing*, vol. 94, pp. 3–20, 2019.
- [11] S. Fortunati, L. Sanguinetti, F. Gini, M. S. Greco, and B. Himed, "Massive MIMO radar for target detection," *IEEE Trans. Sig. Proc.*, vol. 68, pp. 859–871, 2020.
- [12] B. Li, S. Wang, J. Zhang, X. Cao, and C. Zhao, "Fast randomized-MUSIC for mm-wave massive MIMO radars," *IEEE Trans. Veh. Technol.*, vol. 70, no. 2, pp. 1952–1956, 2021.
- [13] A. M. Elbir, K. V. Mishra, and S. Chatzinotas, "Terahertz-band joint ultra-massive MIMO radar-communications: Model-based and model-free hybrid beamforming," *IEEE J. Sel. Topics Signal Process.*, vol. 15, no. 6, pp. 1468–1483, 2021.
- [14] J. Zhang, L. Dai, S. Sun, and Z. Wang, "On the spectral efficiency of massive MIMO systems with low-resolution ADCs," *IEEE Commun. Lett.*, vol. 20, no. 5, pp. 842–845, 2016.
- [15] J. Zhang, L. Dai, X. Li, Y. Liu, and L. Hanzo, "On low-resolution ADCs in practical 5G millimeter-wave massive MIMO systems," *IEEE Commun. Mag.*, vol. 56, no. 7, pp. 205–211, 2018.
- [16] R. Schmidt, "Multiple emitter location and signal parameter estimation," *IEEE Trans. Antennas Propag.*, vol. 34, no. 3, pp. 276–280, 1986.
- [17] Z. Cheng, B. Liao, Z. He, and J. Li, "Transmit signal design for large-scale MIMO system with 1-bit DACs," *IEEE Trans. Wireless Commun.*, vol. 18, no. 9, pp. 4466–4478, 2019.
- [18] Y.-H. Xiao, D. Ramírez, P. J. Schreier, C. Qian, and L. Huang, "One-bit target detection in colocated MIMO radar and performance degradation analysis," *IEEE Trans. Veh. Technol.*, vol. 71, no. 9, pp. 9363–9374, 2022.
- [19] F. Xi, Y. Xiang, S. Chen, and A. Nehorai, "Gridless parameter estimation for one-bit MIMO radar with time-varying thresholds," *IEEE Trans. Sig. Proc.*, vol. 68, pp. 1048–1063, 2020.
- [20] M. Stein, A. Kürzl, A. Mezghani, and J. A. Nossek, "Asymptotic parameter tracking performance with measurement data of 1-bit resolution," *IEEE Trans. Sig. Proc.*, vol. 63, no. 22, pp. 6086–6095, 2015.
- [21] F. Shu, Y. Qin, T. Liu, L. Gui, Y. Zhang, J. Li, and Z. Han, "Low-complexity and high-resolution DOA estimation for hybrid analog and digital massive MIMO receive array," *IEEE Trans. Commun.*, vol. 66, no. 6, pp. 2487–2501, 2018.
- [22] J. An, C. Yuen, C. Xu, H. Li, D. W. K. Ng, M. Di Renzo, M. Debbah, and L. Hanzo, "Stacked intelligent metasurface-aided MIMO transceiver design," *IEEE Wireless Commun.*, vol. 31, no. 4, pp. 123–131, 2024.
- [23] X. Li, Y. Gong, K. Huang, and Z. Niu, "Over-the-air integrated sensing, communication, and computation in IoT networks," *IEEE Wireless Commun.*, vol. 30, no. 1, pp. 32–38, 2023.
- [24] X. Li, F. Liu, Z. Zhou, G. Zhu, S. Wang, K. Huang, and Y. Gong, "Integrated sensing, communication, and computation over-the-air: MIMO beamforming design," *IEEE Trans. Wireless Commun.*, vol. 22, no. 8, pp. 5383–5398, 2023.
- [25] H. Niu, J. An, A. Papazafeiropoulos, L. Gan, S. Chatzinotas, and M. Debbah, "Stacked intelligent metasurfaces for integrated sensing and communications," *IEEE Wireless Commun. Lett.*, vol. 13, no. 10, pp. 2807–2811, 2024.
- [26] S. Li, F. Zhang, T. Mao, R. Na, Z. Wang, and G. K. Karagiannidis, "Transmit beamforming design for ISAC with stacked intelligent metasurfaces," *IEEE Trans. Veh. Technol.*, vol. 74, no. 4, pp. 6767–6772, 2024.
- [27] J. An, C. Yuen, Y. L. Guan, M. Di Renzo, M. Debbah, H. V. Poor, and L. Hanzo, "Two-dimensional direction-of-arrival estimation using stacked intelligent metasurfaces," *IEEE J. Sel. Areas Commun.*, vol. 42, no. 10, pp. 2786–2802, 2024.
- [28] M. Nerini and B. Clerckx, "Analog computing for signal processing and communications—part I: Computing with microwave networks," *IEEE Trans. Sig. Proc.*, 2025.
- [29] —, "Analog computing for signal processing and communications—part II: Toward gigantic MIMO beamforming," *IEEE Trans. Sig. Proc.*, 2025.
- [30] —, "Physics-compliant modeling and optimization of MIMO systems aided by microwave linear analog computers," *arXiv preprint arXiv:2602.19379*, 2026.
- [31] —, "MIMO systems aided by microwave linear analog computers: Capacity-achieving architectures with reduced circuit complexity," *IEEE Trans. Wireless Commun.*, vol. 25, pp. 14597–14610, 2026.
- [32] Q. Zhang, M. Nerini, and B. Clerckx, "Channel estimation in MIMO systems aided by microwave linear analog computers (MiLACs)," *arXiv preprint arXiv:2601.11438*, 2026.
- [33] M. Nerini and B. Clerckx, "Capacity of MIMO systems aided by microwave linear analog computers (milacs)," *arXiv preprint arXiv:2506.05983*, 2025.
- [34] Z. Wu, M. Nerini, and B. Clerckx, "Microwave linear analog computer (MiLAC)-aided multiuser MISO: Fundamental limits and beamforming design," *arXiv preprint arXiv:2601.10060*, 2026.
- [35] T. Fang, X. Zhou, and Y. Mao, "On the performance of lossless reciprocal MiLAC architectures in multi-user networks," *arXiv preprint arXiv:2601.01834*, 2026.
- [36] F. Sohrabi and W. Yu, "Hybrid digital and analog beamforming design for large-scale antenna arrays," *IEEE J. Sel. Topics Signal Process.*, vol. 10, no. 3, pp. 501–513, 2016.
- [37] X. Zhou, T. Fang, Y. Mao, and B. Clerckx, "Two-layer microwave linear analog computer (MiLAC)-aided multi-user MISO networks," *arXiv preprint arXiv:2604.24303*, 2026.
- [38] Y. Peng, Z. Wu, and B. Clerckx, "Hybrid digital and microwave linear analog computer (MiLAC)-aided beamforming for multiuser MIMO-OFDM systems," *arXiv preprint arXiv:2604.26532*, 2026.
- [39] M. Nerini, X. Liu, and B. Clerckx, "Analog computing with hybrid couplers and phase shifters," *arXiv preprint arXiv:2603.24604*, 2026.
- [40] Q. Shi and M. Hong, "Penalty dual decomposition method for non-smooth nonconvex optimization—Part I: Algorithms and convergence analysis," *IEEE Trans. Sig. Proc.*, vol. 68, pp. 4108–4122, 2020.
- [41] P. Heidenreich, A. M. Zoubir, and M. Rubsamen, "Joint 2-D DoA estimation and phase calibration for uniform rectangular arrays," *IEEE Trans. Sig. Proc.*, vol. 60, no. 9, pp. 4683–4693, 2012.
- [42] I. Bekkerman and J. Tabrikian, "Target detection and localization using MIMO radars and sonars," *IEEE Trans. Sig. Proc.*, vol. 54, no. 10, pp. 3873–3883, 2006.
- [43] S. M. Kay, *Fundamentals of statistical signal processing: Estimation theory*. Prentice-Hall, Inc., 1993.
- [44] J. Li, L. Xu, P. Stoica, K. W. Forsythe, and D. W. Bliss, "Range compression and waveform optimization for MIMO radar: A Cramér-Rao bound based study," *IEEE Trans. Sig. Proc.*, vol. 56, no. 1, pp. 218–232, 2007.
- [45] P. H. Schönemann, "A generalized solution of the orthogonal procrustes problem," *Psychometrika*, vol. 31, no. 1, pp. 1–10, 1966.
- [46] M. A. Richards *et al.*, *Fundamentals of radar signal processing*. McGraw-hill New York, 2005, vol. 1.
- [47] S. G. Johnson and M. Frigo, "A modified split-radix FFT with fewer arithmetic operations," *IEEE Trans. Sig. Proc.*, vol. 55, no. 1, pp. 111–119, 2006.
- [48] Z. Yang, L. Xie, and C. Zhang, "Off-grid direction of arrival estimation using sparse bayesian inference," *IEEE Trans. Sig. Proc.*, vol. 61, no. 1, pp. 38–43, 2012.